



ELSEVIER

1 March 2000

OPTICS  
COMMUNICATIONS

Optics Communications 175 (2000) 461–468

www.elsevier.com/locate/optcom

# Compact CH<sub>4</sub> sensor based on difference frequency mixing of diode lasers in quasi-phasematched LiNbO<sub>3</sub>

D.G. Lancaster<sup>a,\*</sup>, R. Weidner<sup>a</sup>, D. Richter<sup>a</sup>, F.K. Tittel<sup>a</sup>, J. Limpert<sup>b</sup><sup>a</sup> *Rice Quantum Institute, Rice University, Department of Electrical and Computer Engineering, 6100 Main Street, Houston, TX 77005-1892, USA*<sup>b</sup> *Institut für Angewandte Physik, Friedrich-Schiller-Universität, Jena, Germany*

Received 20 October 1999; received in revised form 29 December 1999; accepted 29 December 1999

## Abstract

A compact, portable and robust room temperature CH<sub>4</sub> sensor is reported. By difference frequency mixing a 500 mW  $\alpha$ -DFB diode laser at 1066 nm and an erbium-doped fiber amplified 1574 nm DFB diode laser in periodically poled lithium niobate up to 7  $\mu$ W of narrowband radiation at 3.3  $\mu$ m is generated. Real-time monitoring of CH<sub>4</sub> over a 7 day period using direct absorption in an open-path multipass cell ( $L = 36$  m) demonstrates a detection precision of  $\pm 14$  ppb. © 2000 Elsevier Science B.V. All rights reserved.

PACS: 07.57.Ty; 42.65; 07.07.Df; 39.30

Keywords: Difference frequency generation; Molecular spectroscopy; Trace gas detection; Methane

## 1. Introduction

Precise detection and monitoring of trace gases in ambient air using in-situ optical techniques is of considerable importance in applications such as quantifying emitted greenhouse gases, species monitoring for atmospheric chemistry, urban air monitoring and combustion diagnostics.

Almost all molecules have fundamental ro-vibrational absorption lines in the wavelength region from 2 to 20  $\mu$ m, commonly known as the spectroscopic fingerprint region. The near-infrared region (up to 2  $\mu$ m), which can be accessed directly by III–V semi-

conductor diode lasers, is characterized by first and second overtone and combination bands. However, their transition strengths are one to two orders of magnitude weaker than their fundamental absorption lines. This makes the mid-infrared region the choice for high-sensitivity laser absorption spectroscopy.

Difference frequency generation (DFG) is a convenient technique to shift near-infrared telecommunications diode laser sources into the mid-infrared spectral region, particularly if an efficient nonlinear optical material, such as periodically poled lithium niobate (PPLN) is used, which has an optical transparency up to 5  $\mu$ m. By mixing frequency stabilized single-mode diode lasers, robust spectroscopic sources emitting microwatt level radiation in the mid-infrared region can be realized [1–5].

\* Corresponding author. Fax: +1-713-524-5237; e-mail: davelanc@rice.edu

We report the development and preliminary results for a portable  $\text{CH}_4$  gas sensor designed for absolute, sensitive and quasi real-time measurements. The most important requirements to achieve this objective are room temperature operation, compact design, inherent frequency stability, and low optical noise to achieve high absorption sensitivity. Up to  $7 \mu\text{W}$  radiation at  $3.3 \mu\text{m}$  was generated by difference frequency mixing (in PPLN) a  $500 \text{ mW}$   $1066 \text{ nm}$   $\alpha$ -DFB diode laser and a fiber amplified  $1574 \text{ nm}$  DFB diode laser. For the direct absorption spectroscopy monitoring reported here, a multipass cell (open to air) with an effective  $36 \text{ m}$  pathlength is used. The use of fiber delivery and fiber beam combining eliminates alignment and stability issues. This sensor represents our smallest, and simplest yet fiber coupled sensor to date.

A strong motivation to quantify terrestrial methane sources is that this greenhouse gas has been increasing by  $1\%$  per year in the atmosphere [6]. Primary sources include agriculture (particularly rice cultivation), industry, land fills and wetlands. To provide food for an increasing world population, it is predicted that rice farming will continue to rise, for

example rice production in south Asia will need to double over the next 20 years [7], with a corresponding increase in methane emissions if current growth practices are continued. Recent studies [8] have indicated that by the use of genetically modified rice strains and refined growth techniques, methane emissions can be considerably reduced. Hence there exists a need for methane sensors able to monitor methane levels for extended periods over the growth cycle of rice. In addition, ground based sensors are needed to provide ground verification measurements for space based passive remote sensing satellites.

## 2. Experimental configuration

The schematic arrangement of the DFG sensor is shown in Fig. 1. Key components include a mid-infrared laser source, a known absorption pathlength, a mid-IR detector, and a data acquisition and processing system. The entire sensor is assembled on two stacked layers with an overall size of  $25 \times 30 \times 60 \text{ cm}^3$ , a weight of  $23 \text{ kg}$  (including AC to DC power supplies in a separate suitcase) and a power con-

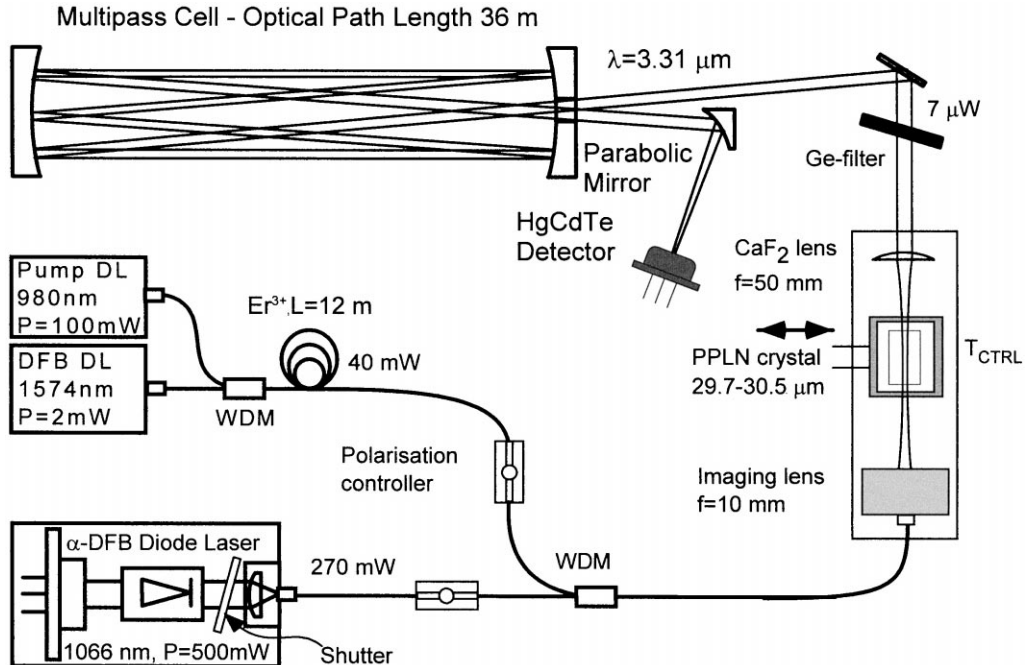


Fig. 1. Schematic of the compact DFG-based gas sensor.

sumption of 60 W. The detector voltage is acquired using a compact PCMCIA 12 bit A-D card, and analyzed on a laptop computer.

The DFG pump source is an  $\alpha$ -DFB diode laser (SDL-6752-P1) with a power of 500 mW at 1066 nm. The beam after passing through an optical isolator ( $-30$  dB isolation) is coupled into single mode fiber with 270 mW being launched into the fiber. This fiber coupling arrangement is mounted on a compact stainless steel bench to ensure rigid coupling. The lower frequency laser is a pigtailed distributed feedback (DFB) telecommunication diode producing 2 mW at 1574 nm. An  $\text{Er}^{3+}$  doped fiber amplifier increases the 1574 nm power to  $\sim 40$  mW. This amplifier consists of  $\text{Er}^{3+}$  doped fiber pumped by a pigtailed 100 mW, 980 nm diode laser. The output power of this telecommunication diode is sufficiently large to saturate this amplifier.

A 1066/1550 nm wavelength division multiplexer (WDM) is used to combine the pump and signal channels into a single mode fiber. In-line polarization controllers in each delivery fiber are employed to set the linear polarization for the  $e + e \rightarrow e$  interaction in PPLN, thereby accessing the highest nonlinear coefficient of lithium niobate ( $d_{33} = 24 \text{ pmV}^{-1}$ ). An antireflection-coated achromatic  $f = 10$  mm lens was used to image the beam spot from the output fiber end (FC-APC) into the 19 mm long, 0.5 mm thick tri-band AR-coated PPLN crystal. The crystal contained 9 quasi-phasematching channels with grating periods ( $\Lambda$ ) from 29.7 to 30.5  $\mu\text{m}$  in 0.1  $\mu\text{m}$  increments. A phasematching condition of  $\Lambda = 30.3 \mu\text{m}$  period at  $27^\circ\text{C}$  was calculated (to generate DFG radiation at  $3028 \text{ cm}^{-1}$ ) using the Sellmeier coefficients for the extraordinary index of refraction ( $n_e$ ) of lithium niobate published by Jundt [9]. The crystal is mounted on a small copper block with an embedded 10 K thermistor, interfaced to a Peltier element to provide temperature regulation. The mid-IR DFG idler beam is collimated by a  $f = 5$  cm plano-convex  $\text{CaF}_2$  lens and the pump and signal beams are blocked by a 3 mm thick AR-coated germanium filter (band gap of 0.66 eV equals  $\lambda \approx 1.9 \mu\text{m}$ ).

To increase the absorption pathlength we employed a  $L = 36$  m multipass cell which was operated with the cell wall removed, hence exposing the beam path directly to ambient air. This cell could

also be used in an extractive configuration with an external pump. The beam emerging from the cell is focused onto a low noise MCT detector by a 30 mm focal-length gold-coated off-axis parabolic mirror. The  $1 \text{ mm}^2$  area MCT detector is operated in a photoconductive mode at a temperature of  $-65^\circ\text{C}$ , achieved by a three stage thermoelectric cooler. The MCT detector is DC-coupled to a low-noise preamplifier with a 3 dB bandwidth of 200 kHz. This was then coupled into a low noise preamplifier (Stanford Research System, Model SR560) with a gain of 10, and a 3 dB bandwidth of 10 kHz. The 1574 nm DFB diode laser was frequency scanned by direct current modulation with a 200 Hz triangular waveform provided by a function generator. The measured modulation function of the 1574 nm DFB is  $-0.03 \text{ cm}^{-1}/\text{mA}$ . A modulation range in excess of  $1.3 \text{ cm}^{-1}$  (39 GHz) allowed monitoring of atmospheric pressure broadened lines. In order to reduce the size of the sensor, compact OEM diode laser current and thermoelectric drivers for the two DFB diodes, 980 nm pump diode and the PPLN crystal are used.

The data acquisition and analysis is controlled by a Labview programmed notebook computer with a PCMCIA 12-bit A-D card, capable of a sampling rate of 500 kS/s. Data acquisition was synchronized to the laser diode modulation by a TTL trigger pulse from the function generator. To acquire a direct absorption spectrum, the laser is repetitively scanned across the lineshape and the amplified detector voltage is acquired by the data acquisition card and averaged. The duty cycle for the data acquisition hardware is typically 50% (on average only every second scan is acquired due to the system overhead). By activating a shutter in the 1066 nm pump beam-path, the detector dark-voltage is obtained which is required for absolute absorption measurements.

### 3. Experimental results

The measured conversion efficiency at  $3.3 \mu\text{m}$  is  $0.75 \text{ mWW}^{-2}$  ( $0.08\%/W$ ), which results in  $7 \mu\text{W}$  (corrected for optical reflection losses in the beam path) of MIR radiation for incident powers of 250 mW and 39 mW in the 1066 nm and 1572 nm DFG pump channels, respectively. After coupling the radiation through the multipass cell,  $0.15 \mu\text{W}$  is incident

on the detector resulting in a measured cell transmission of 3%. This low transmission was attributed to contamination on the cell mirrors. It is expected that after cleaning of the multipass optics the throughput will increase to its specified value of 23%, hence increasing the measured signal to noise on the MCT detector.

A relatively interference free  $\text{CH}_4$  absorption line at  $3028.75 \text{ cm}^{-1}$  was chosen ( $S = 9.519 \times 10^{-20} \text{ cm/molecule}$ ) to demonstrate trace gas monitoring. For accurate calculation of the  $\text{CH}_4$  concentration at atmospheric pressure, close by water lines at  $3028.92 \text{ cm}^{-1}$  and  $3028.238 \text{ cm}^{-1}$  with absorptions of  $\sim 0.1$  of the  $\text{CH}_4$  line need to be taken into account. The presence of several overlapping weaker  $\text{CH}_4$  and

$\text{H}_2\text{O}$  absorption lines (absorptions  $< 0.1\%$ ) introduces a systematic measurement offset estimated to be 3%.

To process the acquired absorption scans a 4-step algorithm was used. In the first step, the portion of the scan representing the absorption peak is removed and a 3rd order polynomial is fitted to the remaining baseline. The polynomial baseline fit is refined in a second step by simultaneously fitting the estimated polynomial with a Lorentzian lineshape to the original spectrum (using a non-linear least squares Levenberg–Marquardt fit). In the third step the detector voltage is normalized to absorption with respect to the acquired detector dark voltage. In the final step, the baseline polynomial function is subtracted from

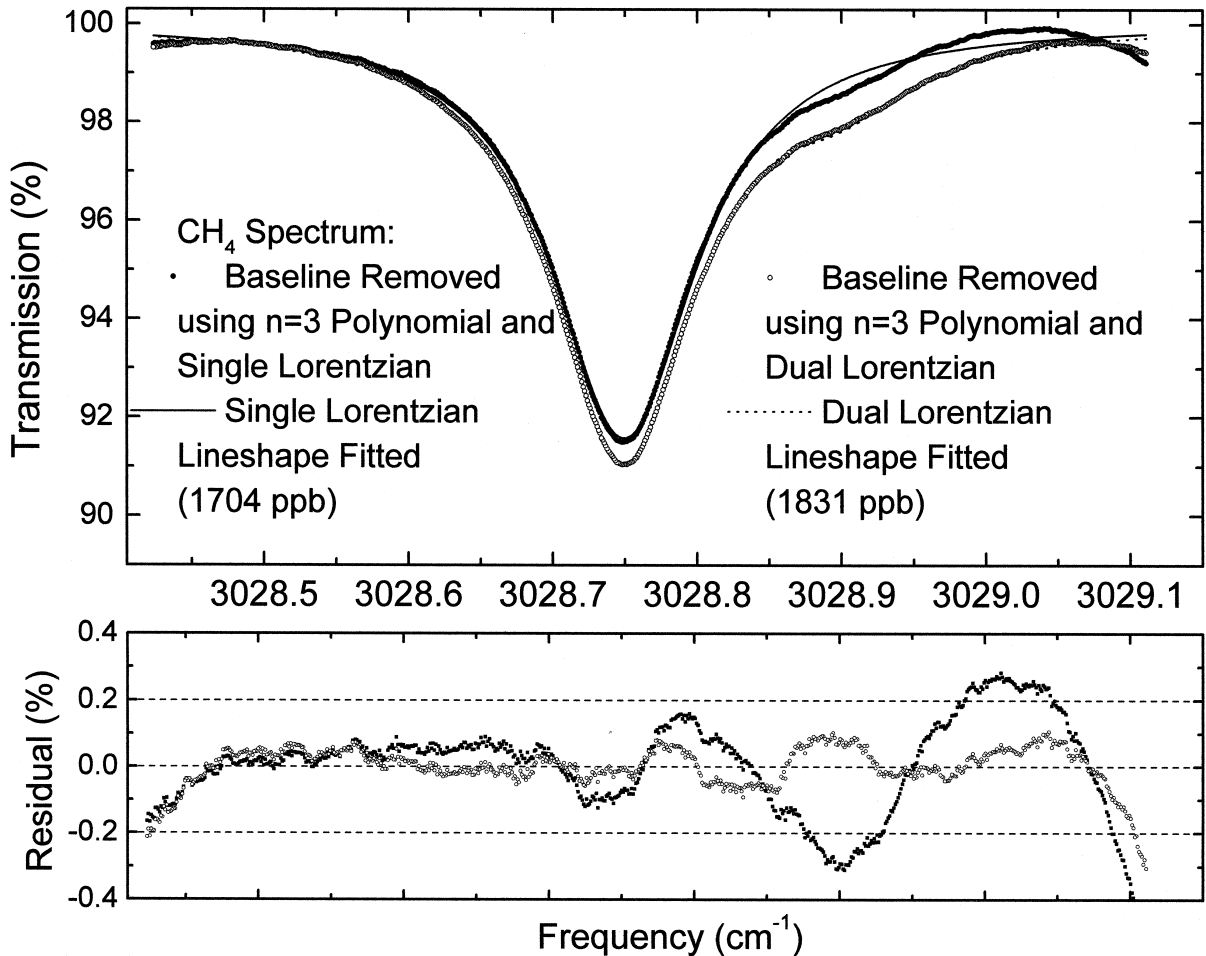


Fig. 2.  $\text{CH}_4$  absorption line at  $3028.75 \text{ cm}^{-1}$  obtained in a  $L = 36 \text{ m}$  open-air absorption path.

the spectrum resulting in a flat baseline, and a Lorentzian lineshape is fitted to the absorption peak. The integrated lineshape area allows the molecular concentration to be calculated. All the data processing and fitting is done in near real-time ( $< 1$  s).

During initial characterization of the sensor the acquired  $\text{CH}_4$  spectrum was processed by fitting a single Lorentzian absorption lineshape, with the weaker  $\text{H}_2\text{O}$  absorption line ( $0.17\text{ cm}^{-1}$  separation) assumed to give a systematic fitting offset. To increase the  $\text{CH}_4$  fitting accuracy and account for changes in the  $\text{H}_2\text{O}$  relative humidity, a dual Lorentzian fit algorithm was subsequently implemented to simultaneously fit the  $\text{CH}_4$  and  $\text{H}_2\text{O}$  absorption lines in both steps 2 and 4.

The upper part of Fig. 2 is an acquired  $\text{CH}_4$  spectrum (500 scan average) in ambient air processed using both the single Lorentzian lineshape

approximation ( $\text{CH}_4$  concentration 1797 ppb) and the more accurate dual Lorentzian lineshape fit (1889 ppb). The same Lorentzian width was used in each case. Fit residuals are shown in the lower part of Fig. 2. The lower  $\text{CH}_4$  concentration calculated from the single peak fit ( $\sim 5\%$  less) is clearly due to the  $\text{H}_2\text{O}$  peak at  $3028.9\text{ cm}^{-1}$  distorting the polynomial baseline estimation. Hence for accurate and absolute  $\text{CH}_4$  concentration measurements at atmospheric pressure this  $\text{H}_2\text{O}$  line should be taken into account. From the residual plot in Fig. 2, it can be seen that the noise on the baseline is noise originating in the detector–preamplifier combination. This indicates that the current sensitivity is not limited by the occurrence of periodic optical fringes arising from etalons caused by the optical elements in the beam path.

To calibrate the sensor a 1773 ppb  $\text{CH}_4$  standard mixture in dry air was monitored (at  $P = 760$  torr)

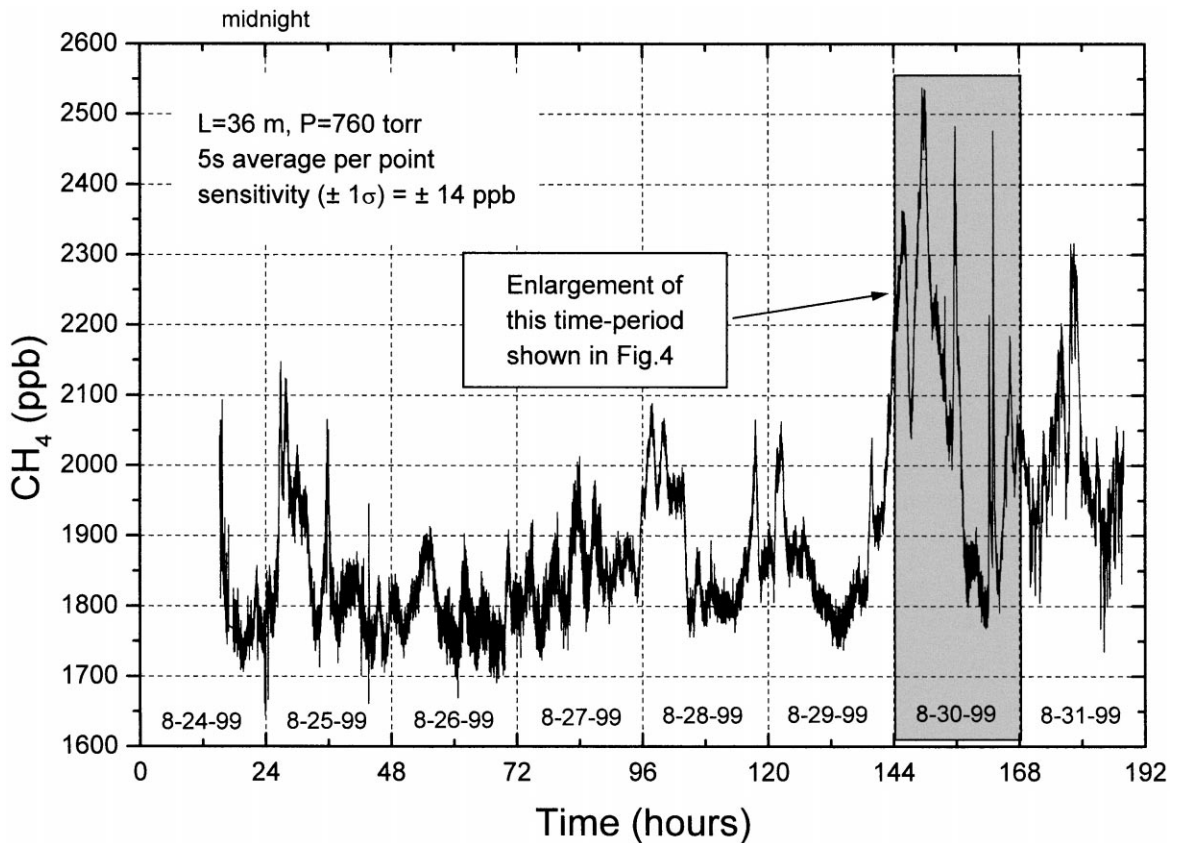


Fig. 3. Calibrated  $\text{CH}_4$  concentration measured over a 7 day period in ambient air.

with the multipass cell connected directly to the calibration cylinder. Using the single line Lorentzian fitting algorithm a  $\text{CH}_4$  concentration of 1843 ppb with a measurement standard deviation of 15 ppb was recorded over a time interval of 60 min (119 measurements) which is within 4% of the calibrated value. The measured concentration offset can be partially attributed to uncertainty in the effective pathlength of the multipass cell that is estimated at  $\pm 2\%$ .

In Fig. 3, the methane concentration measured in the laboratory over 7 days of continuous monitoring is shown. Two  $\text{CH}_4$  measurements were made every minute, with each measurement consisting of averaging 500 individual spectra acquired over 5 s. The individual spectra were not frequency shifted to compensate for laser frequency drift over the acquisi-

tion time as the expected DFG linewidth of  $\sim 0.001 \text{ cm}^{-1}$  [3] is significantly less than the atmospheric broadened  $\text{CH}_4$  absorption linewidth ( $\sim 0.1 \text{ cm}^{-1}$ ). A single Lorentzian-peak fit was used during this work to fit the spectra, but in future work the dual Lorentzian fit procedure as described above will be used. An upward correction of 5% to the  $\text{CH}_4$  concentration was applied to account for the presence of the adjacent water peak. This assumes a constant humidity, and could affect the measured absolute  $\text{CH}_4$  concentration by up to 2%. The overall trend apparent from the data showed significant increases in the methane concentration in room air between mid-night and early in the morning. The presence of personnel in the air-conditioned laboratory during daytime did not noticeably increase ambient  $\text{CH}_4$  concentration levels. Measurement preci-

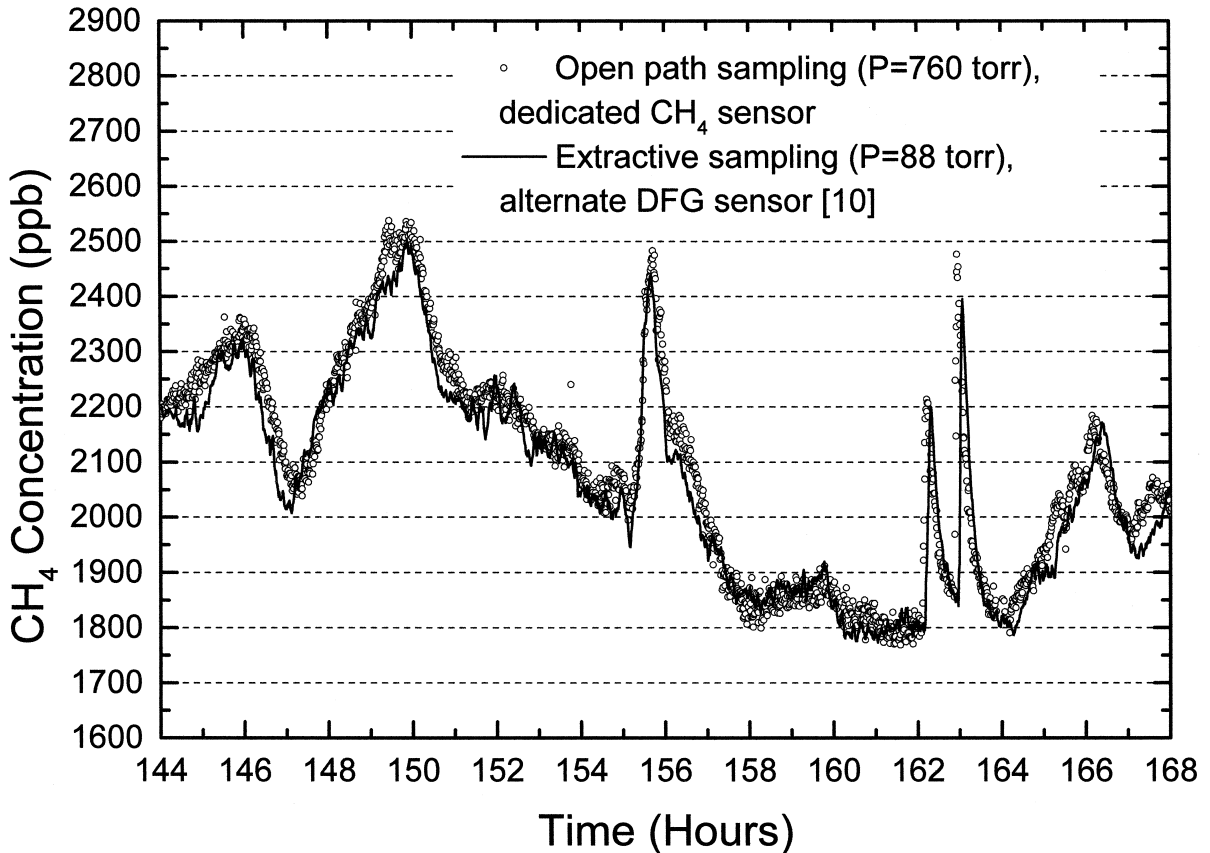


Fig. 4. Comparison of the  $\text{CH}_4$  concentration monitored over a 24 h time period (8-30-99) using both the DFG based sensor reported in this work, and a DFG based multicomponent gas sensor operating at reduced pressure as described in Ref. [11].

sion over the monitoring period was estimated at  $\pm 14$  ppb ( $\pm 1\sigma$ ) by measuring the standard deviation of the recorded concentrations over several short time-periods. A side effect to using the multipass cell with the walls removed is that air movement in the room was found to introduce low frequency variations of the detected power. This was attributed to beam steering by subtle refractive index variations caused by the moving air and reduced considerably by use of wind-blocks placed adjacent to the cell.

To provide an independent verification of the measured CH<sub>4</sub> level and trends, a separate DFG-based multispecies sensor [10] was operated in an alternative configuration that employed reduced pressure extractive sampling at 88 torr. The main advantage of the reduced pressure is a reduction in the pressure broadening of the spectral lines, thereby allowing CH<sub>4</sub> and H<sub>2</sub>O spectral lines to be clearly resolved and more accurately fitted. This sensor was placed adjacent to the CH<sub>4</sub> sensor to allow comparative measurements. Fig. 4 is 24 h of comparative CH<sub>4</sub> concentration data measured independently by each sensor, showing close agreement between the two DFG based gas sensors.

Over the course of the experiment, no sensor realignment or polarization adjustment was required. Minor adjustments included reoptimizing the set point temperature for the PPLN crystal due to temperature induced drift of the reference resistance (attributed to the sensor base-plate warming up over the course of the experiment). In addition the temperature set point of the 1574 nm diode laser was also adjusted twice (by  $\sim 0.3$  cm<sup>-1</sup>) to compensate for drift of the MIR frequency from the center of the scan window. The detector voltage bias was also adjusted several times to keep the detector output voltage within the optimum A-D voltage range ( $\pm 1$  V).

Low frequency detector and preamplifier noise currently limit sensitivity as the incident power on the detector is relatively low at 180 nW. It is expected that with more power incident on the detector, the sensitivity will improve by a similar factor. Furthermore it was apparent in this experiment that the sensitivity was limited by low frequency oscillations occurring in the detector dark-voltage ( $< 0.1$  Hz). Acquiring the detector dark voltage both before and after a CH<sub>4</sub> spectrum was acquired reduced the magnitude of this low frequency noise.

By use of additional discrete DFB telecommunications diode lasers, or an external cavity diode laser tunable around  $\sim 1550$  nm, several other important species can be monitored such as formaldehyde and HCl. In future work it is envisaged that this sensor will be made more autonomous by use of feedback to the DFB diode controller to continuously ensure that the spectral line of interest is kept within the scan range. In addition by modulating at higher frequencies (2–5 kHz), and improving the data acquisition rate and scan processing time, fast sub second measurements of CH<sub>4</sub> will be possible, which will allow eddy correlation measurements of methane fluxes [11].

#### 4. Summary

A portable fiber-coupled narrow bandwidth DFG-based trace gas sensor generating up to 7  $\mu$ W in the spectroscopically important mid-infrared region has been demonstrated. This new DFG based sensor architecture is relatively simple and difference frequency mixes a 0.5 W  $\alpha$ -DFB diode laser at 1.066  $\mu$ m with an Er<sup>3+</sup> fiber amplified DFB telecommunications diode laser in the 1.57  $\mu$ m region selected for a specific trace gas species. The long-term stability has been verified by monitoring the CH<sub>4</sub> concentration in ambient air over a 7 day period with a precision of 28 ppb ( $\sim 1.5\%$ ), and the absolute accuracy is estimated to be within 5%.

#### Acknowledgements

This research was supported by NASA, the Texas Advanced Technology Program, the Welch foundation and the National Science Foundation.

#### References

- [1] K.P. Petrov, L. Goldberg, W.K. Burns, R.F. Curl, F.K. Tittel, *Opt. Lett.* 21 (1996) 86–88.
- [2] T. Töpfer, K.P. Petrov, Y. Mine, D. Jundt, R.F. Curl, F.K. Tittel, *Appl. Opt.* 36 (1997) 8042–8049.
- [3] D.G. Lancaster, D. Richter, R.F. Curl, F.K. Tittel, *Appl. Phys. B* 67 (1998) 339–345.

- [4] L. Goldberg, J. Koplow, D.G. Lancaster, R.F. Curl, F.K. Tittel, *Opt. Lett.* 23 (1998) 1517–1519.
- [5] D.G. Lancaster, L. Goldberg, J. Koplow, R.F. Curl, F.K. Tittel, *Electron. Lett.* 34 (1998) 1345–1346.
- [6] P. Steele, E.J. Dlugokencky, P.M. Lang, P.P. Tans, R.C. Martin, K.A. Masarie, *Nature* 358 (1992) 313–316.
- [7] R. Sass et al., *Ecol. Bull.* 42 (1992) 199–206.
- [8] R.L. Sass, F.M. Fisher, S.T. Lewis, M.F. Jund, F.T. Turner, *Global Biogeochem. Cycles* 8 (2) (1994) 135–140.
- [9] D.H. Jundt, *Opt. Lett.* 22 (1997) 1553–1555.
- [10] D.G. Lancaster, D. Richter, F.K. Tittel, *Appl. Phys. B* 69 (1999) 459–465.
- [11] P. Werle, *Europta*, 1999, in press.